Autogenous Yb:YAG laser disk welding domain of AA6061-T4 aluminium alloy

Ameth Faye[1], Yannick Balcaen[2], Loic Lacroix[3], Joel Alexis[4]

Université de Toulouse, LGP, ENIT/INPT, 47 av. d'Azereix, BP1629, 65016 Tarbes cedex, France

Abstract— *The aerospace industry is developing lighter, stronger and more heat- and corrosion-resistant components to reduce manufacturing costs and fuel consumption. To achieve this goal, laser welding represents a real opportunity to replace the riveting assemblies developed in the 1920s. In this article, we present our research to obtain the weldability domain of AA6061 aluminium alloy by autogenous disk laser welding. A systematic study of the samples butt-welded by X-ray and optical microscopy allowed us to determine the defects and the dimensions of the weld beads according to the process parameters. The data analysis with the CORICO software made it possible to determine the regression models considering the welding parameters in order to avoid the appearance of defects such as melt pool collapse, lack of penetration or hot cracking. A range of weldability was defined for power values between 2000 to 2500 W, welding speeds below 4m/min and focal diameters below 170 microns.*

Keywords— *aluminium alloy, laser welding, weldability domain.*

I.   INTRODUCTION

Since the beginning of the 21st century, the share of organic matrix composite materials has increased considerably in aircraft structures [1]. In order to remain competitive for the manufacture of new single-aisle aircraft, new metal alloys or new solutions for using these alloys will have to be developed. Concerning aluminium alloys, which remain key alloys for the aeronautical field, two solutions for joining by friction stir welding or laser welding seem promising to replace the riveting assemblies developed in the 1920s. These complementary processes result in weight savings by eliminating excess thickness or sealant and productivity gains [2–4].

Concerning more specifically laser welding, there are nowadays several laser sources such as CO_2 lasers or solid-state lasers (fiber or disc). CO_2 sources have been implemented faster in the industry because they were more powerful and cheaper. The advent of the new disc sources allows for higher quality, higher power and lower cost solid state laser beams [5,6]. In addition, their shorter wavelength compared to CO_2 lasers reduces reflection problems when welding alloys such as aluminium alloys [7]. Indeed, the physical and chemical characteristics of high-strength aluminium alloys lead to welding difficulties that must be considered in the welding procedures. The most frequently encountered problems are the difficulty to obtain sufficient penetration depths, correct bead geometries, weld beads without porosity and cracks. Insufficient penetration of the fusion zone is due to insufficient laser beam energy during welding. Geometrical defects such as undercut or incomplete fusion can be generated when welding speeds are too high [8]. Hot cracking occurs at the end of the solidification of the alloy when the dendritic skeleton is not sufficiently formed to resist deformation and the permeability of the liquid medium is very low. At this stage, the material has low strength and low ductility. In order to limit this susceptibility to hot cracking, Hu et al. propose to optimize welding parameters, to reduce thermal contraction stresses by preheating or by modifying the chemical composition of the molten bath with a filler metal [9]. The small porosities are due to the low miscibility of hydrogen in the solid state of aluminium alloys [10]. The presence of hydrogen in the liquid bath during welding is due to poor surface preparation [11]. Large porosities can also exist in welds. They result from instability of the keyhole during the welding phase [12]. The extent of these weld defects depends, among other things, on the welding parameters, hence the need to study the influence of each parameter on the characteristics of the weld [13]. In this study, the weldability range of AA6061-T4 alloy, without filler metal, was investigated using an Yb: YAG source.

II.   MATERIALS AND METHODS

2.1   Sample welding conditions

The samples were butt welded, without filler metal, using a 3. 3 kW Yb:YAG disc laser source on a TruLaser Cell 3000 five-axis laser machine. The emitted beam is guided by a 2-in-1 coaxial optical fiber. The focal diameter can therefore vary from 120 μm to 370 μm for the Core Fiber (CF) and from 450 μm to 750 μm for the Outer Fiber (OF). The power density is distributed in Gaussian form for the CF and annular for the OF [7,14]. The clamping system allows the samples to be maintained edge to edge, with precise positioning of the parting line (Fig. 1). The shielding gas on the reverse side sweeps along the entire length of the bead, in the opposite direction to the welding direction. The primary chamber is designed to contain the metal vapors from the weld bead under gas protection. The bottom of the secondary chamber consists of a copper reflector, which reflects the fraction of the beam that can possibly pass through the weld bead towards the wall of this chamber.
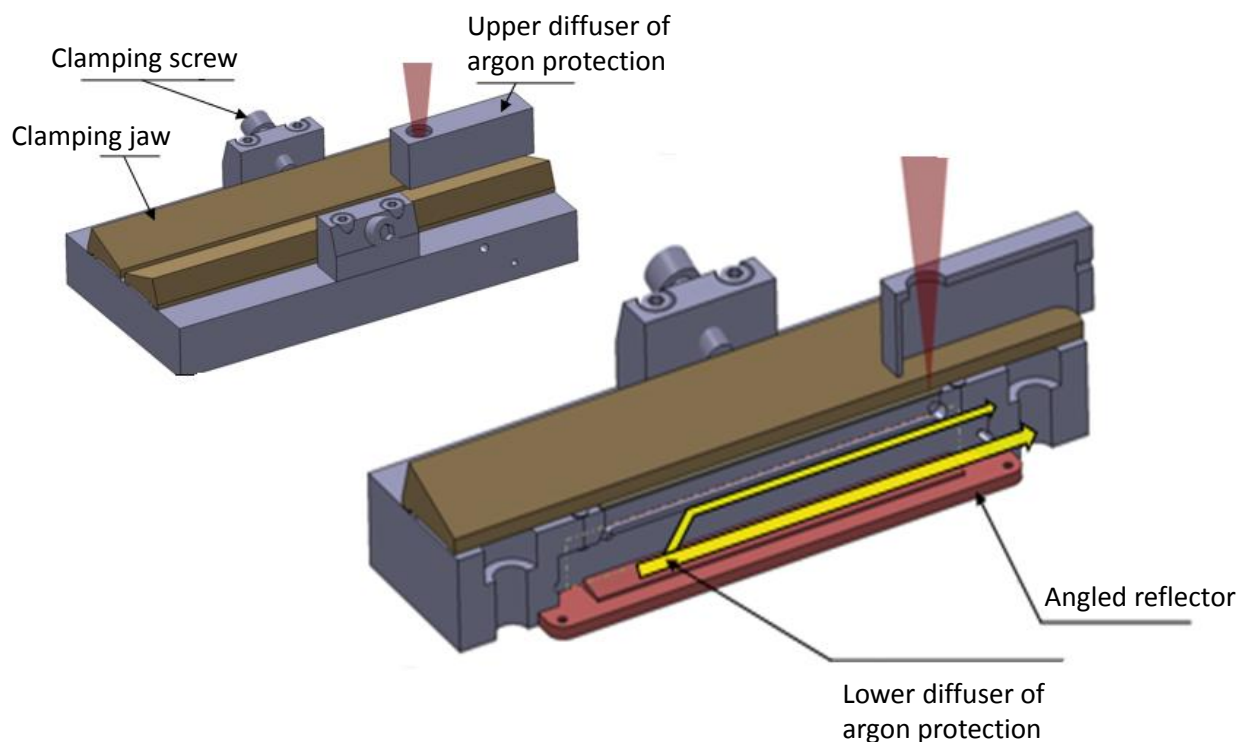
FIGURE 1: Experimental set-up to weld AA6061 aluminium alloy samples

The surface preparation followed before welding consists in mechanical stripping (sanding with P600 SiC paper) to renew the alumina layer, removing other hydroxide compounds that may form on the surface of the material. This step is followed by degreasing and cleaning of the surface of the part using acetone. The surface preparation aims to promote weldability but also to guarantee a good internal bead health (porosities, oxide inclusions). To make the preparation effective, the welding is carried out shortly (less than an hour) after preparation.

The study of the influence of parameters such as beam power, welding speed, the focal point diameter on the bead geometry, on the porosity and cracking was carried out for both fiber configurations (Table 1). In order to limit the number of samples while trying to obtain as much information as possible between process parameters and bead characteristics, experimental designs were generated for each fiber from the CORICO[TM] software[15]. 108 samples were welded for this study (36 with the OF and 72 with the CF). Other operating parameters are set such as the position of the focal point in relation to the sheet metal surface, the nature and flow rate of the gas for upper and lower weld protection or the surface preparation of the AA6061 sheet metal (Table 2).

<div align="center">

TABLE 1
VARIABLE OPERATING PARAMETERS OF THE STUDY

</div>

Beam power (W)	500 to2500
Welding speed (m/min)	1 to 8
Focal diameter (µm)	120 to 370 (core fiber) 450 to 750 (outer fiber)

<div align="center">

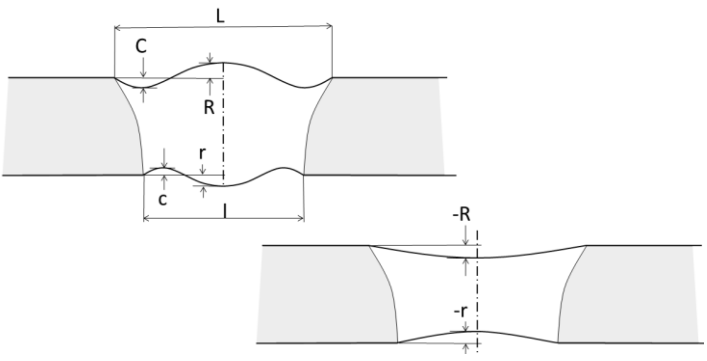**TABLE 2**
FIXED PARAMETERS DURING THE WELDING OPERATION

</div>

Position of the focal point relative to upper the surface	Protective gas: Nature / gas flow rate	
	Upper protection	Lower protection
0. 3 mm	Argon / 40l/min	Argon / 20 l/min

2.2   Methods for characterizing welds

All the weld beads were first studied by non-destructive methods. Radiographic observations were carried out for the analysis of volume defects (porosities) or plane defects (cracks) using the Easytom RX Solution tomograph. The acquisition parameters used are a voltage of 115 kV and a current of 260 µA. These analyses were supplemented by metallographic observations in transverse section in order to determine the morphology and dimension of the welds as a function of the operating parameters. The validation of the beads is based on the acceptance criteria for welds of aluminium alloy parts defined by the NF L 06-395 2010. Based on these criteria, a weldability range of the 1mm-thick AA6061-T4 alloy welded with the Yb: YAG laser has been determined (Table 3).

<div align="center">

TABLE 3
GEOMETRICAL CRITERIA FOR WELD SEAMS ACCORDING TO THE NF L06-395 2010 STANDARD.

</div>

| Defect	Symbol	Dimensions (mm)		
Face width:	L	2	maxi	
Face concavity:	-R	-0. 1	mini	
Face reinforcement:	R	0. 3	maxi	
Face undercut:	C	0. 15	maxi	
Root width	l	1. 5	maxi	
Root concavity:	-r	-0. 1	mini	
Root reinforcement	r	0. 4	maxi	
Root undercut	c	0. 1	maxi	

<div align="center">

III.   RESULTS AND DISCUSSION

</div>

3.1   Weldability domain

3.1.1   Bath collapse and weld penetration

The collapse of the molten pool and the pronounced lack of penetration were observed by light microscopy on some beads (Fig. 2). Of the 108 samples, 39 weld beads showed a penetrating weld without melt pool collapse (36 with CF and 3 with OF). Collapse is generally observed when the power density of the laser beam is excessive ($>10^7$ W/cm^2) and/or the interaction time is greater than 5. 5 10^{-3}s. This defect is only encountered with the core fiber configuration, where power density levels are very high (up to 2 10^7 W/cm^2). In this case, it is preferable to decrease the beam power or increase the focal diameter. The lack of penetration is, on the contrary, usually caused by low beam power and/or high welding speed. The high thermal diffusivity of aluminium and its alloys as well as their high reflection due to the brightness of their surface favors these risks of fusion lack of the edges to be joined by preventing the necessary absorption of heat to melt the parts to be

welded. This defect type, mainly driven by the beam power density, strongly limits welding with the large fiber of the TruLaser Cell 3. 3 kW center where, due to the large focal diameter, the power density of the beam does not exceed 1. 5 10^6 W/cm^2. More than 91 % of the beads welded using outer fiber present penetration defect.
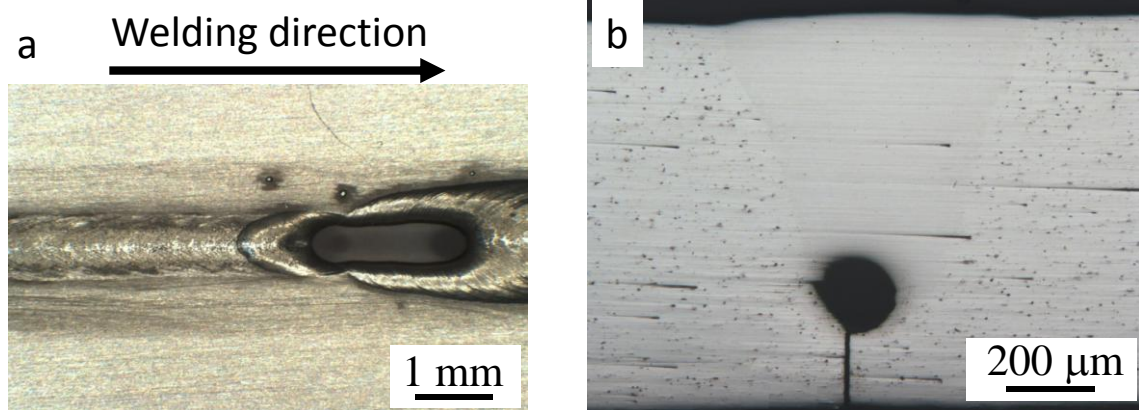

FIGURE 2: Optical observations with defects in the welds: (a) face view of molten pool collapse (P = 2000 W, V = 2. 75 m/min, Øf = 305 µm), (b) Cross section evidencing lack of penetration and associated root porosity (P = 2500 W, V = 4. 5 m/min,Øf = 600 µm)

Cords with both good penetration and no collapse were radiographed to investigate the possible presence of porosities and cracking.

3.1.2   Porosity and cracking

X-ray analysis revealed a few microporosities averaging about 60 µm in size in some welds (Fig. 2). However, no cracks or macroporosities were observed on the pre-selected welds for tomographic analysis. Optical microscopic observations of metallographic sections confirmed the presence of pores with a diameter of about 15 µm (Fig. 4a). Cracks were also observed in the fusion zone of the welds obtained with the outer fiber (Fig. 4b). The welding of AA6061 with the outer fiber is therefore limited by the lack of penetration and cracking. Nevertheless, the welds made with a small focal diameter (CF) are all free of cracking. As a reminder, according to the NF L 06-395 2010, no crack, whatever its size, is tolerable in a weld of an aluminium part. In conclusion, a range of weldability exists for AA6061 alloy by laser welding Yb:YAG without filler metal.
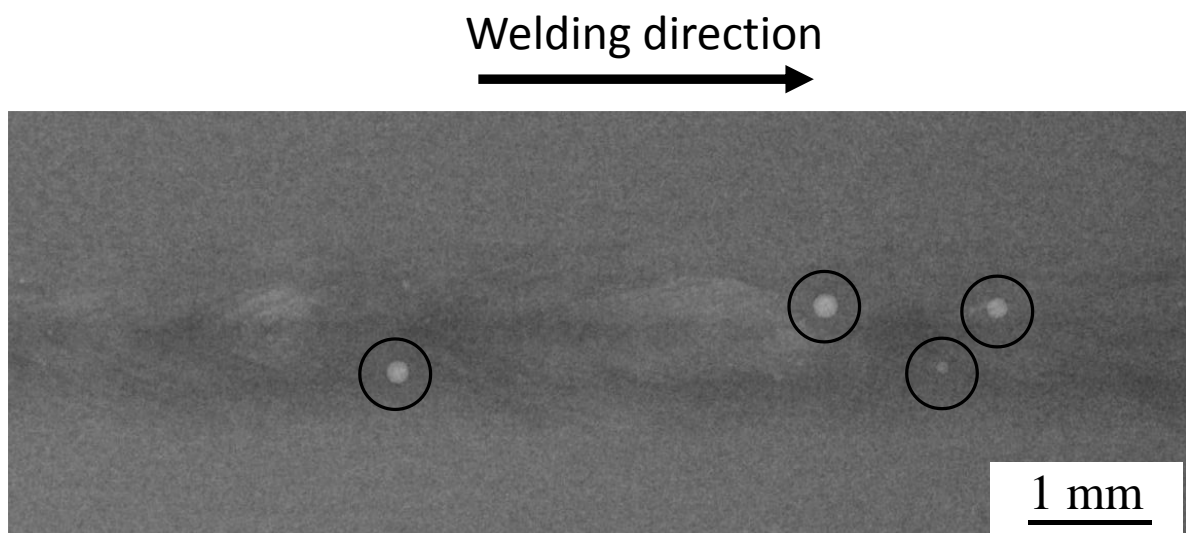
FIGURE 3: X-ray radiographic observation showing microporosities in the fusion zone of a weld (P = 2230 W, V = 3. 7 m/min, Øf = 153 µm)
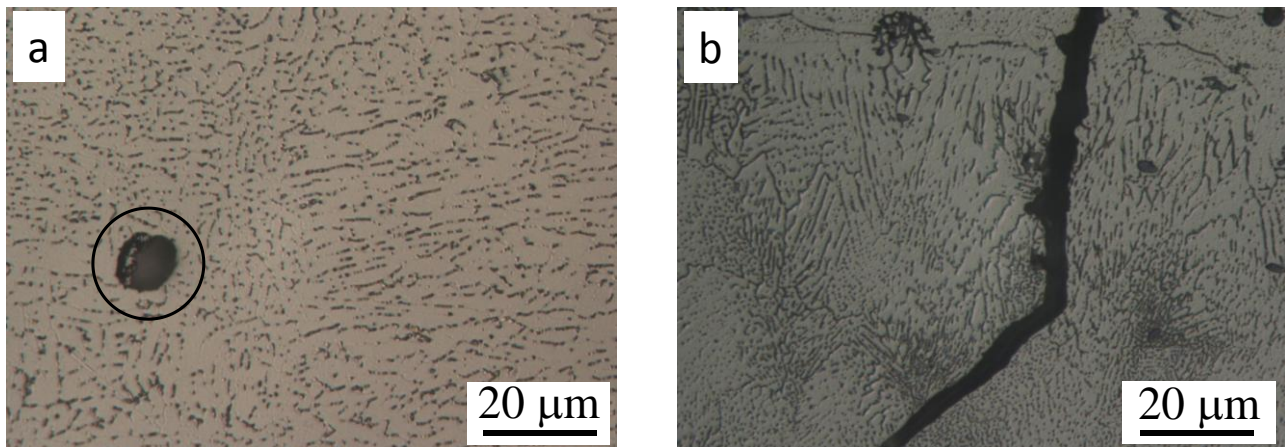
FIGURE 4: Optical micrographs showing (a) porosity (P = 2000 W, V = 2. 27 m/min, Øf = 134 µm) and (b) cracking in the fusion zone of a weld (P = 2500 W, V = 2. 5 m/min, Øf = 675 µm)

3.1.3   Geometry weld defects

Dimensional limits for specific common imperfections and shape dimensions in laser beam fusion welding are also measured to verify weld bead conformance. The figure 5 shows different shapes of weld beads in cross section. In spite of good penetration and the absence of porosity and cracking, geometrical defects may appear at the base or on the right side of the weld beads. Such defects generally constitute areas of crack initiation but also concentration of internal stresses that weaken the part. They are therefore prohibited. Approximately 23% of CF fiber specimens without porosities or cracks have a geometry defect. This weld cross-sectional irregularity is observed, in most cases, when the power density is greater than 10^6 W/cm^2 and the interaction time is less than 510^{-3} s. This corresponds to a range of high power and high welding speed leading to instability of the molten pool. This phenomenon is facilitated by the thermal properties of the alloy.
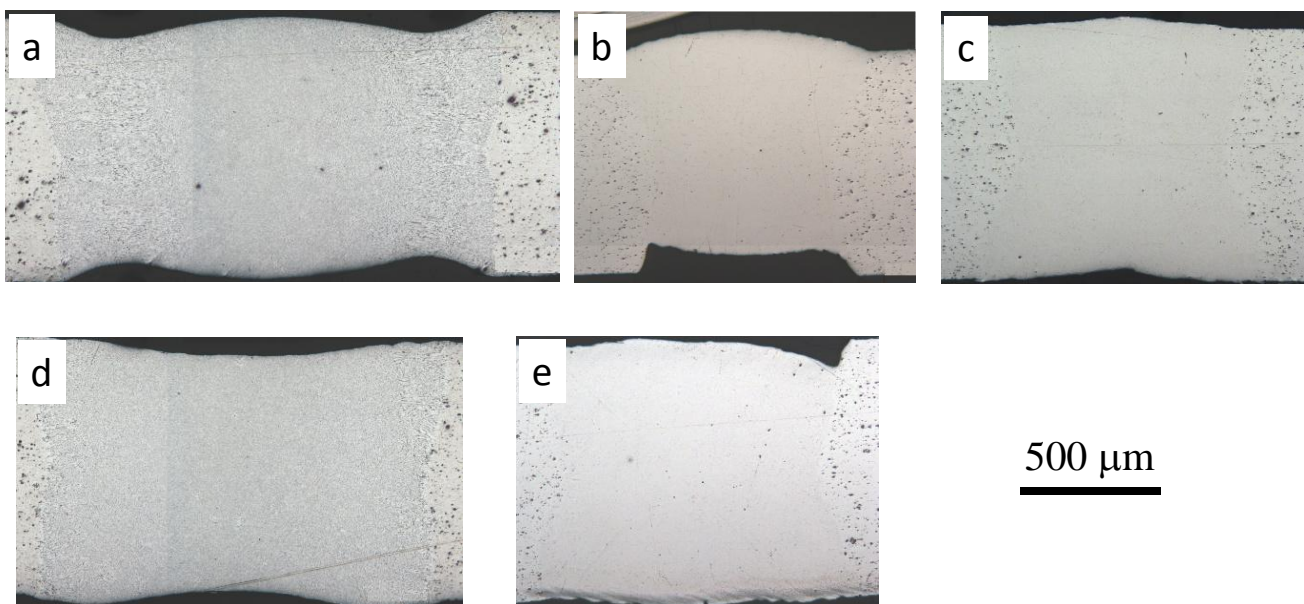
FIGURE 5: Non-conforming weld bead micrographs:(a) P = 900 W, V = 7. 05 m/min,Øf = 195µm, (b)P = 2500 W, V = 8 m/min, Øf = 370 µm, (c)P = 1000 W, V = 2. 75 m/min, Øf = 240 µm(d)1000 W, V = 6. 25m/min, Øf = 175 µm, (e)P = 2000 W,V = 8 m/min, Øf = 305 µm.

Among all the welded samples, only 26 were able to meet the above-mentioned standard requirements. This corresponds to slightly less than 25% of the full experimental design. The weldability range of the 1 mm thick alloy AA6061-T4 welded by laser beam Yb: YAG according to the criteria chosen in this study is shown in Figure 6. This weldability range is defined at power densities between $5\ 10^6$ and $2\ 10^7$ W/cm^2 and an interaction time lower than $6\ 10^{-3}$ s. Only the core fiber allows welding this alloy thanks to the high-power densities lJof the laser beam. Welding with the outerfiber is limited by penetration and hot cracking defects. Indeed, with the outerfiber, the power densities do not allow to melt the whole thickness of the part to be assembled, without generating excessively wide beads, presenting hot cracking.
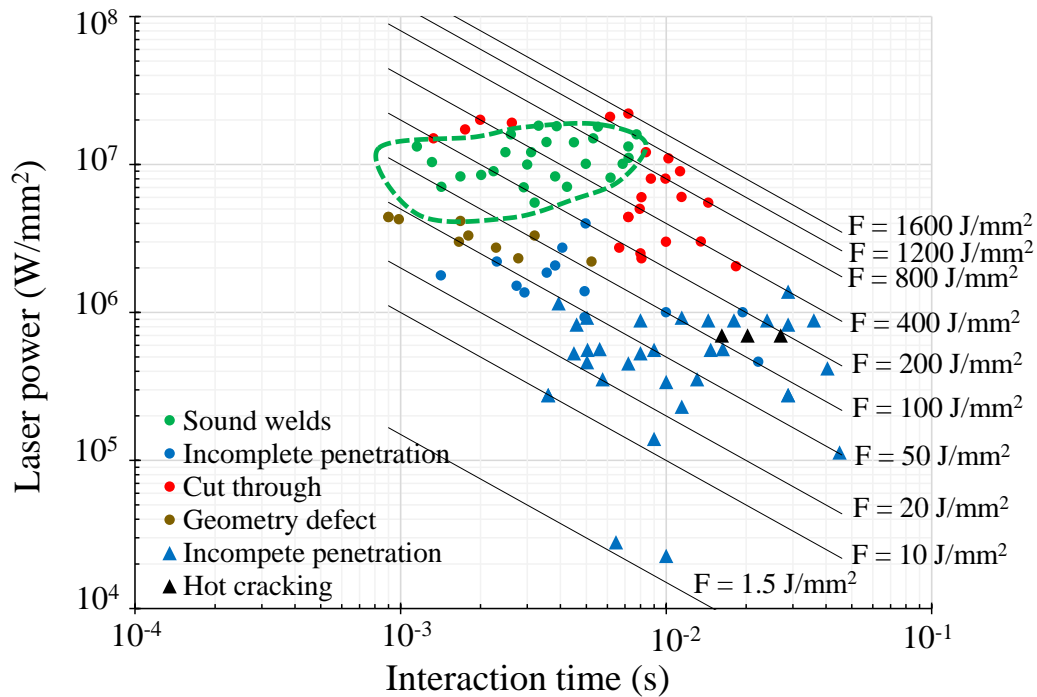
FIGURE 6: Weldability domain of AW6061-T4 welded by Yb: YAG laser

3.2   First order process parameters

The presentation of the weldability range as a function of power density and interaction time cannot be used directly to weld AA6061-T4 alloy. It is necessary to decouple each operating parameter (laser power, welding speed and diameter at the focal point) to determine their influence on the weldability criteria chosen in this study, i. e. penetration, bead geometry, melt pool collapse or cracking. To reach this objective, we determined the iconographic sphere of the correlations between the laser parameters and the weldability criteria (Fig. 7).
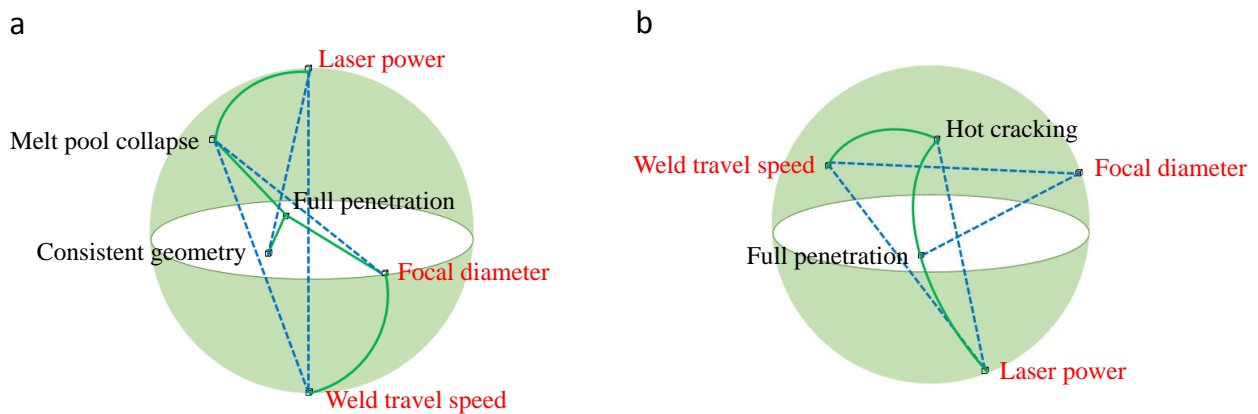

FIGURE 7: Iconographic correlation spheres for Yb: YAG laser welding of alloy AA6061-T4: (a) core fiber, (b) outer fiber

In the correlation iconography, solid lines indicate a positive correlation and dashed lines indicate a negative correlation. The smaller the distance between the factor and the response, the greater the contribution of that factor. For the welds obtained with the core fiber, only the power of the laser beam has a positive correlation with the collapse of the molten pool. In fact, an increase in the beam power leads to the difficulty of stabilizing the keyhole and therefore the possibility of having a melt bath collapse or incorrect geometry beads. An increase in welding speed reduces the susceptibility to melt pool collapse. An increase in focal diameter improves weld penetration. Indeed, the power density becomes excessive when the focal diameter is very small and under these conditions the molten pool collapse becomes almost inevitable. We can say that for laser welding with small fiber, every process parameter has a strong influence on welding problems such as melt pool collapse, lack of penetration and non-conformity of the bead geometry. For a good quality weld, an optimum choice of these

parameters seems to be necessary. For welds obtained with the outer fiber, a minimum power density is necessary to obtain sufficient penetration of the beads. This can be achieved mainly by increasing the beam power or by decreasing the focal point diameter. On the other hand, an increase in cord penetration is accompanied by the risk of hot cracking. This risk is increased with an increase in welding speed [16].

The response areas for obtaining a conformal weld bead with the core fiber are given in Figure 8. To obtain compliant weld beads, the process parameters must be within the following ranges: power between 2000 and 2500 W, focal diameter less than 170 μm and welding speed less than 4 m/min.
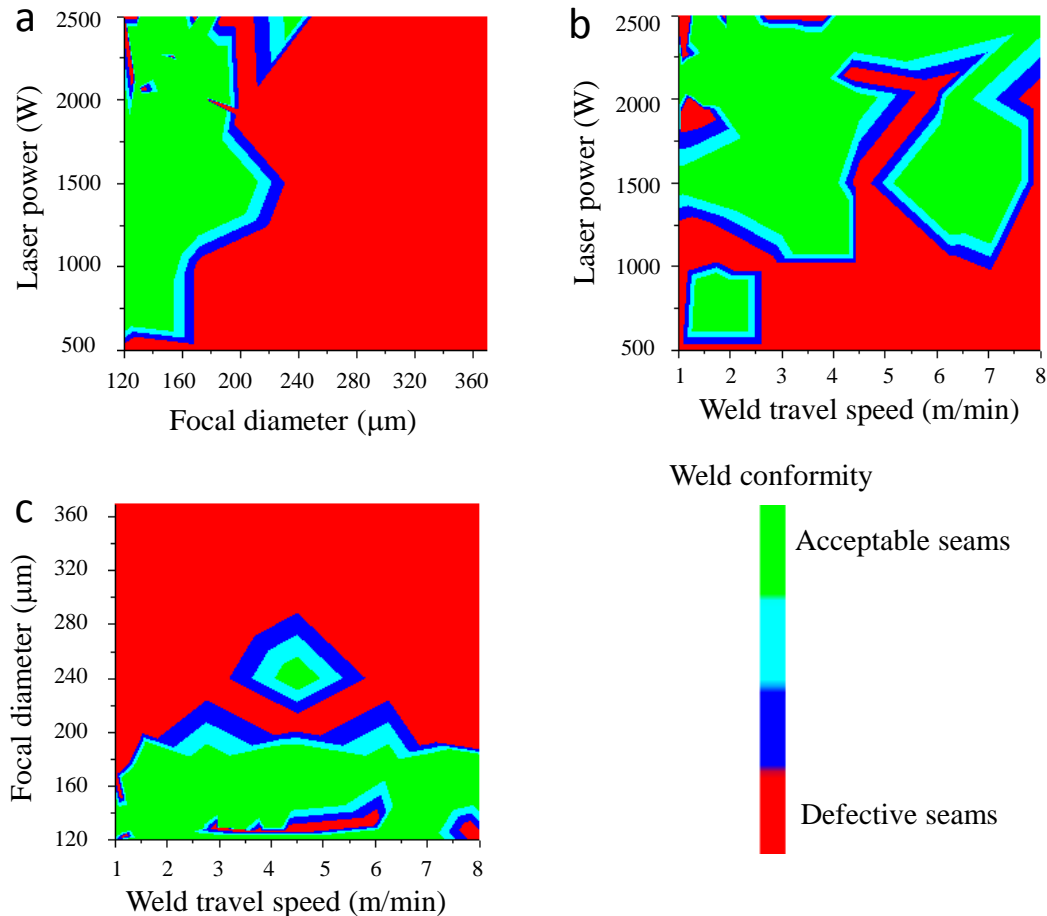
FIGURE 8: Response surfaces showing the effect of weld parameter interaction on weld conformance

Correlation analysis and regression modelling were obtained using CORICO software for each response (Table 4). The regression model was defined to find the model with the smallest standard error. The CORICO model accounts for logical interactions in the equations. The meaning of each logical interaction in the equations presented is as follows:

- X1&X2 means that Y is high when the value of both X1 and X2 are high,

- X1^X2 means that Y is high when the value either or both X1 and X2 are high,

- X1&-X2 means that Y is high when the value of X1 is high and X2 is low,

- X1-X2 means that Y is high when the difference between X1 and X2 is high,

- X1]X2 means that Y correlates with X1 when X2 is high,

- X1#-X2 means that Y is high when X1 did not vary as X2,

- X1{X2 means that Y is high when X1 is at average and X2 is high,

- X1{-X2 means that Y is high when X1 is at average and X2 is low.

TABLE 4

REGRESSION MODELS FOR EACH RESPONSE AS A FUNCTION OF THE LOGICAL INTERACTIONS OF FACTORS.

Regression models	Correlation coefficient (R)
Core fiber	
Compliant weld = 0. 3611 + 2. 015 Power{-Focal diameter - 0. 8425 Focal diameter{Focal diameter + 1. 111 Power]Speed + 0. 8686 Speed}Focal diameter + 0. 6850 Power!Speed	0. 74
Collapse of the weld bead = 0. 3194 - 1. 914 Speed^Speed + 1. 243 Power]Focal diameter+ 1. 338 Focal diameter{Focal diameter- 0. 9791 Focal diameter]Speed	0. 62
Non-Compliant geometry = 0. 8611 - 1. 506 Speed]Speed - 0. 8527 Speed!Focaldiameter+ 0. 8442 Power]Speed	0. 72
Full penetration = 0. 8194 - 2. 069 Focal diameter&-Power + 0. 9730 Power!Focaldiameter+ 0. 7047 Power&-Power - 0. 6033 Speed&-Speed - 0. 5955 Focal diameter{- Power - 0. 3990 Speed#Focal diameter	0. 83

IV.   CONCLUSION

Laser welding of thin sheet is particularly interesting for aero-structures manufacturers. This work, focused on 1mm thick AA 6061 T4 alloy, allowed determining the processing window in autogenous laser welding, by mean of a dense experimental design. Sound weld is obtained with relatively high power densities, between $5 \ 10^6$ and $2 \ 10^7$ W/cm^2 and an interaction time lower than $6 \ 10^{-3}$ s. Within this domain, porosities diameters remain under 15 µm, no cracks are observed, and weld seams cross sections show a standard compliant geometry. Regression models are proposed for determination of weldability window, but also to describe appearance of main defects. Based on this study, further work will be focused mechanical properties and corrosion behavior of these assemblies.

REFERENCES

[1]   X. Zhang, Y. Chen, J. Hu, Recent advances in the development of aerospace materials, Progress in Aerospace Sciences. 97 (2018) 22–34. https://doi. org/10. 1016/j. paerosci. 2018. 01. 001.
[2]   N. Kashaev, V. Ventzke, G. Çam, Prospects of laser beam welding and friction stir welding processes for aluminum airframe structural applications, Journal of Manufacturing Processes. 36 (2018) 571–600. https://doi. org/10. 1016/j. jmapro. 2018. 10. 005.
[3]   M. C. Chatervedi, ed. , Welding and joining of aerospace materials, Woodhead Publishing, Cambridge, UK : Philadelphia, PA, 2012.
[4]   A. A. Gialos, V. Zeimpekis, N. D. Alexopoulos, N. Kashaev, S. Riekehr, A. Karanika, Investigating the impact of sustainability in the production of aeronautical subscale components, Journal of Cleaner Production. 176 (2018) 785–799. https://doi. org/10. 1016/j. jclepro. 2017. 12. 151.
[5]   A. Giesen, J. Speiser, Fifteen Years of Work on Thin-Disk Lasers: Results and Scaling Laws, IEEE J. Select. Topics Quantum Electron. 13 (2007) 598–609. https://doi. org/10. 1109/JSTQE. 2007. 897180.
[6]   G. Verhaeghe, B. Dance, An assessment of the welding performance of high-brightness lasers and a comparison with in-vacuum electron beams, in: International Congress on Applications of Lasers & Electro-Optics, Laser Institute of America, Temecula, California, USA, 2008: p. 710. https://doi. org/10. 2351/1. 5061340.
[7]   J. Alexis, J. D. Beguin, P. Cerra, Y. Balcaen, Yb: YAG Laser Welding of Aeronautical Alloys, MSF. 941 (2018) 1099–1104. https://doi. org/10. 4028/www. scientific. net/MSF. 941. 1099.
[8]   O. O. Oladimeji, E. Taban, Trend and innovations in laser beam welding of wrought aluminum alloys, Weld World. 60 (2016) 415–457. https://doi. org/10. 1007/s40194-016-0317-9.
[9]   B. Hu, I. M. Richardson, Mechanism and possible solution for transverse solidification cracking in laser welding of high strength aluminium alloys, Materials Science and Engineering: A. 429 (2006) 287–294. https://doi. org/10. 1016/j. msea. 2006. 05. 040.
[10] M. Tiryakioğlu, Solubility of hydrogen in liquid aluminium: reanalysis of available data, International Journal of Cast Metals Research. 32 (2019) 315–318. https://doi. org/10. 1080/13640461. 2020. 1718337.
[11] X. Zhang, T. Huang, W. Yang, R. Xiao, Z. Liu, L. Li, Microstructure and mechanical properties of laser beam-welded AA2060 Al-Li alloy, Journal of Materials Processing Technology. 237 (2016) 301–308. https://doi. org/10. 1016/j. jmatprotec. 2016. 06. 021.
[12] D. Rasmussen, Étude sur la fissuration à chaud de l'alliage 6061 lors du soudage par procédé hybride laser-GMAW /, Université du Québec à Chicoutimi, Chicoutimi, 2008. https://doi. org/10. 1522/030043965.
[13] J. C. Ion, Laser beam welding of wrought aluminium alloys, Science and Technology of Welding and Joining. 5 (2000) 265–276. https://doi. org/10. 1179/136217100101538308.
[14] J. Graneix, J. -D. Beguin, J. Alexis, T. Masri, Influence of Yb:YAG Laser Beam Parameters on Haynes 188 Weld Fusion Zone Microstructure and Mechanical Properties, Metall and Materi Trans B. 48 (2017) 2007–2016. https://doi. org/10. 1007/s11663-017-0989-6.
[15] J. Graneix, J. -D. Beguin, F. Pardheillan, J. Alexis, T. Masri, Weldability of the superalloys Haynes 188 and Hastelloy X by Nd:YAG, MATEC Web of Conferences. 14 (2014) 13006. https://doi. org/10. 1051/matecconf/20141413006.
[16] F. Dausinger, R. Fabbro, D. Grevey, G. Peix, P. Peyre, A. B. Vannes, Caractérisation, modélisation et maîtrise des porosités créées lors du soudage laser Nd-YAG d'alliages d'aluminium, (n. d.) 174.